Highly absorbent cellulose nanofibrils aerogels prepared by supercritical drying

Clémentine Darpentigny, Guillaume Nonglaton, Julien Bras, Bruno Jean

Highly Absorbent Cellulose Nanofibrils Aerogels Prepared by Supercritical Drying

Clémentine DARPENTIGNY,[1,2,3] Guillaume NONGLATON,[1] Julien BRAS*[,2] and Bruno JEAN[3]
[1] Univ. Grenoble Alpes, CEA, LETI, MINATEC Campus, F-38054 Grenoble, France
[2] Univ. Grenoble Alpes, CNRS, Grenoble INP, LGP2, F-38000 Grenoble, France
[3] Univ. Grenoble Alpes, CNRS, CERMAV, 38000 Grenoble, France.
Corresponding author: Julien.bras@grenoble-inp.fr - + 33 (0)4 76 82 69 15

Abstract

In this paper, strictly speaking aerogels of cellulose nanofibrils (CNFs) and TEMPO-oxidized CNFs (TO-CNFs) were obtained from an optimized supercritical drying processes and cryogels were prepared after freeze-drying. The cryogels and aerogels were characterized and the influence of the preparation process on the resulting properties was studied. Significant differences were observed in the micro- and nanoscale organization of the porous structures. In addition, the specific surface areas measured varied from 25 to 160 $m^2.g^{-1}$ for CNF materials, depending on the preparation process. Very high specific surface areas up to 482 $m^2.g^{-1}$ among the highest reported for pure cellulose nanofibrils porous materials were achieved for TO-CNF aerogels. Finally, in order to evaluate their aptitudes for wound dressings applications, the capillary water uptake capacities were assessed on skin mimicking layers. From this study, it was revealed that TO-CNF aerogels can absorb almost 120 times their own weight of water.

Keywords: cellulose nanofibrils; aerogels; cryogels; supercritical drying; water uptake

Abbreviations:

AFM: atomic force microscopy

BET: Brunauer, Emmett et Teller

CNFs: cellulose nanofibrils

DLVO: Derjaguin, Landau, Verwey, and Overbeek

NMR: nuclear magnetic resonance

PBS: phosphate buffered saline

SEM: scanning electron microscopy

TEM: transmission electron microscopy

TEMPO: (2,2,6,6-tetramethylpiperidin-1-yl)oxidanyl

TO-CNFs: TEMPO-oxidized cellulose nanofibrils

1. Introduction

Cellulose nanofibrils (CNFs) also called nanofibrillated cellulose are a class of bio-based and versatile materials extensively studied (Klemm et al., 2018; Nechyporchuk, Belgacem, & Bras, 2016). They are commonly extracted from plants after mechanical treatments. Chemical (TEMPO oxidation) (Saito, Nishiyama, Putaux, Vignon, & Isogai, 2006) or enzymatic (M. Pääkkö et al., 2007) pre-treatments are used as supplementary extraction procedure to ease the defibrillation. The long and entangled nanofibrils obtained present a versatile range of applications, from the food industry to cosmetics as rheology modifiers, in paper and packaging, nanocomposites and their biocompatibility makes them attractive materials for biomedical applications (Jorfi & Foster, 2015). Their bioavailability, renewable characters, added to their commercial availability and reactivity owing to the presence of hydroxyls groups contribute to increase their great interest.

Cryogels and aerogels of nanocellulose are studied for their low density, high specific surface area and porosity, with applications in energy storage, heat insulation, selective filtration, biomedical field, *etc*. (Han, Zhang, Wu, & Lu, 2015; Nyström et al., 2015; Stergar & Maver, 2016; Zhou et al., 2016). In the biomedical field, nanocellulose porous materials are investigated for drug delivery, wound care dressing or tissue engineering, often after functionalization. The main challenge of the preparation of porous materials is to preserve the high porosity and low density. Nanocellulose porous foams are classically prepared by means of two distinct drying processes namely freeze-drying and supercritical drying. Because of the difference of morphology generated by the different processes, it is necessary to use adequate terminology, as demonstrated by Buchtová and Budtova (2016). Porous foams obtained from freeze-drying will be called cryogels and those obtained from supercritical drying, aerogels. In both cases, the liquid-vapor interface is avoided, therefore diminishing the capillary pressure during solvent removal.

Freeze-drying involves a first step of freezing, followed by the removal of the solid solvent by sublimation. The freezing step is of particular importance and the different processes and speeds of freezing the nanocellulose suspension result in varied morphologies (Martoïa et al., 2016; Zhang, Yu, Jiang, & Wang, 2015). Solvent exchange to *tert*-butyl alcohol (*t*BuOH) prior to freeze-drying has been used to better preserve the porous organization. The use of *t*BuOH reduces the capillary pressure during the freeze-drying process, giving rise to porous materials with higher specific surface areas

and more fibrillary networks (Fumagalli, Sanchez, Molina Boisseau, & Heux, 2013; Jin, Nishiyama, Wada, & Kuga, 2004; Sehaqui, Zhou, & Berglund, 2011).

Another method to reach high specific surface areas is supercritical drying. It implies a systematic solvent exchange step to a solvent miscible with carbon dioxide, commonly ethanol or acetone. Solvent exchange with liquid CO_2 takes place at low temperature and high pressure before reaching the supercritical state. Mild supercritical parameters of temperature and pressure can be used with carbon dioxide, that need to be heated higher than 31°C and compressed higher than 74 bars to reach the supercritical state. The liquid to gas phase interphase is bypassed by reaching the supercritical state and therefore allowing a better architecture control. This technique is used to prepare bacterial cellulose (Liebner et al., 2010), CNCs (Buesch, Smith, Eschbach, Conley, & Simonsen, 2016; Heath & Thielemans, 2010) and CNF aerogels. Korhonen et al. (2011) prepared cryogels and aerogels of CNFs to be further used as template for the design of inorganic hollow nanotubes. By comparing the two processes, the microscopic observation revealed less interfibrillary aggregation in CNF aerogels contrary to CNFs cryogels. Ciftci et al. (2017) prepared cryogels and aerogels from lupin hull CNFs and they compared aerogel to cryogels prepared from a suspension in water. Differences of morphology, porosity and specific surface area were observed, with aerogel resulting in higher porosity, open porous network and higher specific surface areas. The thermal diffusivity of cryogels and aerogels of oxidized CNFs was investigated by Sakai et al., (2016). Differences in morphology and specific surface area were reported as well.

In this study, we compare cellulose nanofibrils and TEMPO-oxidized CNF porous structures obtained from freeze-drying of suspensions in water and in *tert*-butyl alcohol and aerogels obtained from an optimized supercritical drying process. The macro- and microscale morphologies are investigated and we show the effect of the process and the nature of the nanocellulose particles on the pore size distributions. The effect of three variables, namely the process, the concentration and the type of nanocellulose, on the specific surface area is investigated. In order to assess the potential use of these materials for biomedical and wound dressings applications, the water uptake capacities after immersion in water or phosphate-buffered saline (PBS). Skin phantoms layers were then developed and a more accurate and realistic investigation of the capillary water uptake of the various structures was performed on skin mimicking layers.

2. Materials and methods

2.1.1. Chemicals

Tert-butyl alcohol (≥99.0 %, CAS number: 75-65-0) was purchased from Fisher Scientific and used without any further purification. Ethanol absolute anhydrous (64-17-5, RSE for electronic use) was purchased from Carlo Erba Reagents. Phosphate buffered saline (CAS: 7778-77-0, 10X) was purchased from Fisher Scientific and diluted 10 times before use. Gelatin (CAS Number: 9000-70-8, from porcine skin) and agar powder (CAS Number: 9002-18-0, microbiology grade) used to prepare skin mimicking layers and were purchased from Sigma-Aldrich.

2.1.2. Cellulose nanofibrils (CNFs)

Cellulose nanofibrils were provided by Borregaard (Exilva P) at 2 wt. % or 10 wt. % solid content. Redispersion at required concentration was performed before use during 5 minutes with an Ultra Turrax IKA T25 stirrer at 8000 rpm.

2.1.3. TEMPO-oxidized CNFs

TEMPO-oxidized CNFs (TO-CNFs) were purchased from Centre Technique du Papier (CTP, Grenoble, France) at 2 wt. % solid content. Redispersion at required concentration was performed before use during 5 minutes with an Ultra Turrax IKA T25 stirrer at 8000 rpm.

2.2. Sample preparation

2.2.1. Solvent exchange

Solvent exchange to *t*BuOH was performed by centrifugation-dispersion cycles. A suspension of CNFs was centrifuged at 11200 rpm during 30 minutes at room temperature. The supernatant was discarded and the pellet redispersed in *t*BuOH at 30°C. Following centrifugations took place at 30°C to avoid freezing of tert-butyl alcohol. Four cycles of centrifugation-dispersion were necessary and the last pellet was dispersed in tBuOH/H_2O 80:20 (vol/vol).

Prior to supercritical drying, CNFs were solvent exchange to ethanol after successive soaking in water/ethanol mixtures inside a PTFE mold of 1 cm in height and 1 cm in diameter, perforated with 1 mm wide holes and supplemented with a nylon sieve of 1 µm. Successive soakings of 1 hour with increasing ratios of ethanol/water (25 %, 50 %, 75 %, 100 %) were performed. The last soaking in absolute ethanol was repeated twice during 24 hours.

2.2.2. Freeze-drying

Cryotec® shelves lyophilizer were used for the freeze-drying of the CNF or TO-CNF suspensions. The suspension was poured in cylindrical molds where the suspension was in direct contact with the freeze-drier shelves at -50°C. Directional freezing occurred at -50°C for 2 hours. The primary freeze-drying step took place at 0.1 mbar with increasing temperature from -50°C to 20°C in 24 hours. The secondary freeze-drying step was performed at 20°C and 0.01 mbar for 30 minutes, after which cryogels were recovered and stored in a nitrogen cabinet.

2.2.3. Supercritical drying

The supercritical drying was performed using the SFD-200 equipment built by SEPAREX (Nancy, France) and 31Degrees (Montauban, France). After solvent exchange to ethanol, the molds containing the nanocellulose suspension were placed in a 450 mL pressurized chamber. The chamber was thermo-regulated at 18°C and pressurized liquid CO_2 was introduced to reach a pressure of 100 bars, at a speed of 20 bars.min^{-1}. Ethanol was replaced with liquid CO_2 after successive static baths of 1 hour, in between which liquid CO_2 was flushed and replaced. After three baths, the temperature was increased to 45°C, so that carbon dioxide reaches the supercritical state. After 1 hour, the pressure was decreased at a pace of 8 bars.min^{-1}. A total amount of 0.75 kg of L-CO_2 was necessary.

2.3. Characterizations

2.3.1. Cellulose nanofibrils nanoscale fraction

The nano-sized fraction of the suspension was estimated as explained in a quality index specifically developed for cellulose nanofibrils (Desmaisons, Boutonnet, Rueff, Dufresne, & Bras, 2017). The nanoscale particles were also isolated from the CNFs suspension after centrifugation of a 0.02 % suspension at 1000 rpm during 15 minutes. The supernatant was recovered and considered to be composed of nanoscale particles only. At least triplicates were performed.

The nanoscale fraction (%) was defined as $\frac{Concentration\ after\ centrifugation\ (wt.\%)}{Concentration\ before\ centrifugation\ (wt.\%)}\ x\ 100$

2.3.2. NMR analysis

Solid-state ^{13}C NMR were acquired with a Bruker Avance DSX 400 MHz spectrometer in cross-polarization and magic angle spinning conditions (CP-MAS), at a spinning speed of 12000 Hz. A minimum number of 10 000 scans were acquired, at 100.6 MHz with an acquisition time of 35 ms and a sweep width of 29 400 Hz. Spectra were corrected with the scaling factor obtained from a reference spectrum of glycine. The spectra were normalized with cellulose C1 peak at 100 to 110 ppm. The degree of crystallinity was calculated from the ratio of crystalline (87 to 93 ppm) over

amorphous (80 to 87 ppm) peaks of carbon 4. The degree of oxidation was estimated from the peak at 170-180 ppm corresponding to the C6 in carboxylate groups.

2.3.3. Electron microscopy

The cellulose nanofibrils suspensions were observed with a Philips CM200 CRYO TEM transmission electron microscope (TEM) operating at 80 kV. One drop of diluted suspension was deposited on a carbon grid and excess liquid was removed. A 2 % uranyl acetate stain was deposited on top of the samples, excess liquid was removed after 2 minutes and the sample was allowed to dry before negative staining observation. The macro-sized fraction of the CNF suspension was observed using a Zeiss Axioplan 2 optical microscope and images were recorded with an Olympus SC50 digital camera operated by the Olympus Stream software.

A FEI Quanta 250 scanning electron microscope (SEM) equipped with a field emission gun and operating at 2 kV was used to record CNF and TO-CNF cryogels and aerogels images, after sample coating with gold/palladium.

2.3.4. Image analysis

Particles sizes were measured from electron and optical microscopy images using the ImageJ software. The average values of length and width correspond to measurements of at least 150 particles.

Pore sizes were measured from SEM images of central parts of cryogels and aerogels, at x250 magnification on a surface area of 65 000 µm² and at x800 magnification on a surface area of 20 000 µm².

2.3.5. Nitrogen adsorption

Specific surface area was studied using a Micromeritics ASAP 2420 Surface Area and Porosity Analyzer. Around 100 mg of cryogel or aerogel were degassed at 105°C during at least 12 hours. Nitrogen adsorption and desorption was performed at -196°C and full isotherms were acquired. Specific surface area analysis was calculated with the Brunauer, Emmett, Teller (BET) method (Brunauer, Emmett, & Teller, 1938). Specific surface area measurements were performed in triplicate for each sample.

2.3.6. Shrinkage

The volume of the obtained cryogel or aerogel was measured using digital calipers. Volume shrinkage was measured as follows:

$Shrinkage = \frac{V_{initial} - V_{final}}{V_{initial}} \times 100$, with $V_{initial}$ the suspension volume, corresponding to the volume of the mold and V_{final} the volume of the dry cryogel or aerogel.

2.3.7. Water uptake

Around 5 mg of cryogel or aerogel were placed in a recipient with 5 mL of water or phosphate buffered saline (PBS) at room temperature. After 48 hours of soaking, the structure was weighted. The water uptake, sometimes defined as the swelling ratio, was defined as follows:

$Water\ uptake\ (wt./wt.) = \frac{m_{wet} - m_{dry}}{m_{dry}}$, with m_{wet} the mass of the wet structure and m_{dry} the mass of the structure before immersion. At least duplicates were performed.

Capillary water uptake

The preparation of skin mimicking layers was adapted from Chen et al. (2016). They were composed of a dermis mimicking layer and an underneath hypodermis-mimicking layer to prevent drying effect. First, the hypodermis layer was prepared by mixing 2 % gelatin and 0.2 % agar in distilled water. Microwave heating was applied during 30s to obtain a homogeneous solution. The warm solution (around 40°C) was poured into a mold to reach 15 mm thickness and left to dry for 30 minutes. The dermis layer was prepared similarly with 24 % gelatin and 1 % agar and was poured when hot over the hypodermis layer to reach a thickness of 5 mm. After cooling, cylindrical cryogels and aerogels were placed on the dermis-mimicking layer at room temperature and 50 % relative humidity. The mass of cryogel and aerogel was reported at previously determined times and the water uptake was calculated as previously described. At least triplicates were performed.

3. Results and Discussion

Two types of commercial CNFs were used in this study and the suspension photographs and TEM images are presented in Fig. 1. The first type is a commercial source of CNFs obtained from wood pulp and will be referred to as CNFs. The second type consists of TEMPO-oxidized nanofibrils, which will be called TO-CNFs. Because of the different processes used to produce them and because of their different chemistries, CNFs and TO-CNFs exhibit very different morphologies. The suspension of CNFs appears as a non-transparent and grey-white viscous suspension. When looking at optical microscopy images, we can observe individual fibers with an average length of 9 µm, and bundles of packed microfibrils (supplementary material, Fig. A1). The nanoscale fraction was determined gravimetrically after centrifugation of a highly diluted suspension and revealed that 34 % of the particles are nano-sized. Analysis of TEM micrographs showed the nanoscale fibrils in the CNF suspension have an average length higher than 1700 nm and a width of 25 ± 14 nm. The TO-CNF

suspension appears as a transparent gel. From electron microscopy images, we note the greater homogeneity of the TO-CNFs which are 255 ± 104 nm long and 4 ± 1.4 nm wide, with a narrow width polydispersity. TO-CNFs have a carboxylic content of 1 mmol.g^{-1} (deduced from ^{13}C solid-state NMR spectra acquisition, supplementary material, Fig. A2b). Because of the electrostatic repulsion due to the negatively charged carboxyl groups, the suspension is colloidally stable.

Both types of nanofibrils are semi-crystalline, and their degree of crystallinity has been determined by ^{13}C NMR analysis (supplementary material, Fig. A2a and b). Commercial CNFs have a crystallinity of 49 % and TEMPO-oxidized CNFs have a crystallinity of 42 %. Such difference in crystallinity is due to the source of cellulose being different and not the process as it has been shown that TEMPO-oxidation does not impact the crystalline degree of cellulose (Besbes et al. 2011, Saito and Isogai 2004).

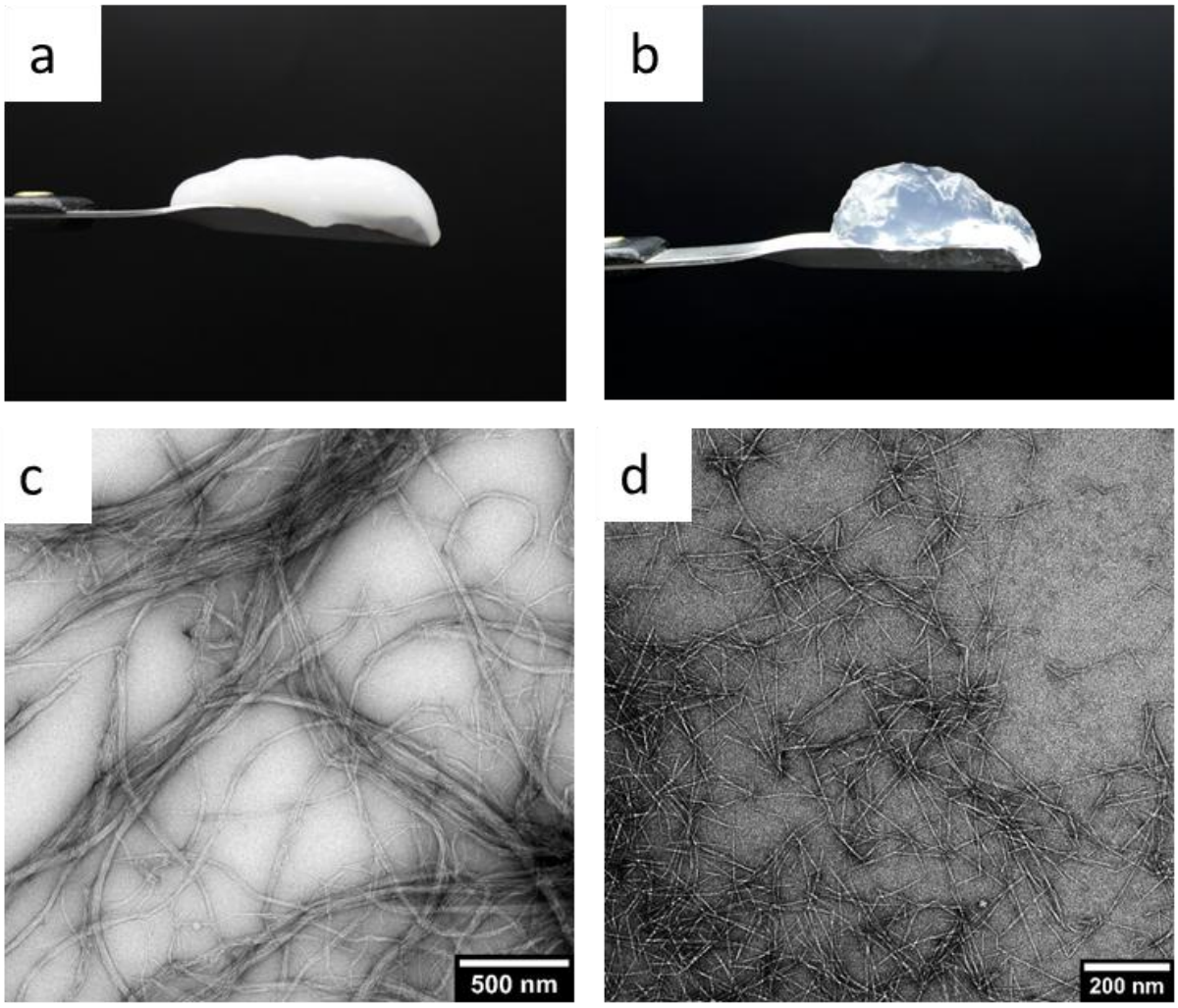

Fig. 1 Photographs (a and b), transmission electron microscopy images (c and d) of CNF suspension (right) and TO-CNF suspension (left).

3.1. Supercritical drying: process optimization

Aerogels production involves an initial step of solvent exchange to a solvent miscible with water and carbon dioxide. Ethanol was selected and once the cellulose nanofibrils have been solvent exchanged they were placed inside the pressurized chamber where liquid carbon dioxide (L-CO_2) was introduced. After several flushing with liquid CO_2, the temperature was increased to reach the supercritical state. Finally, the pressure was decreased and porous aerogels (AG) were recovered.

First experiments were performed at high depressurization rate and resulted in cracks and collapse in the aerogels structures. Indeed, during aerogel production, the depressurization rate is thought to be the main cause of shrinkage (Sanz-Moral, Rueda, Mato, & Martín, 2014) due to the carbon dioxide expansion. Therefore, the depressurization was set to a relatively low rate of 8 bars.min^{-1} in this study.

Supercritical drying can be carried out with either a continuous flow of scCO_2 or batches of static scCO_2 (García-González, Camino-Rey, Alnaief, Zetzl, & Smirnova, 2012; Heath & Thielemans, 2010; Liebner et al., 2010). In order to reduce the amount of carbon dioxide used, the drying is performed under static conditions in this study.

For the first step of solvent exchange from ethanol to liquid CO_2, the effect of the number of liquid cycles and therefore the amount of L-CO_2 injected was investigated. One cycle in L-CO_2 is considered to be the complete replacement of L-CO_2 inside the pressurized chamber. First experiments were carried out with L-CO_2 cycles lasting 6 hours each. However, in order to develop a time-efficient procedure, this time was reduced to 1 hour. In the preparation of aerogels, it is the number of cycles in a liquid CO_2 state that appears to have a strong impact on the macroscale morphology. Indeed, when this number of steps is below three, incomplete drying (for 0 and 1 cycle) and important collapse and shrinkage higher than 90 % is observed and reported in Fig. 2. This is correlated to the amount of solvent remaining adsorbed on the CNF surface that can lead to shrinkage. When a third L-CO_2 cycle is performed, remarkable improvement of the aerogel structure is observed and shrinkage is reduced to 48 %.

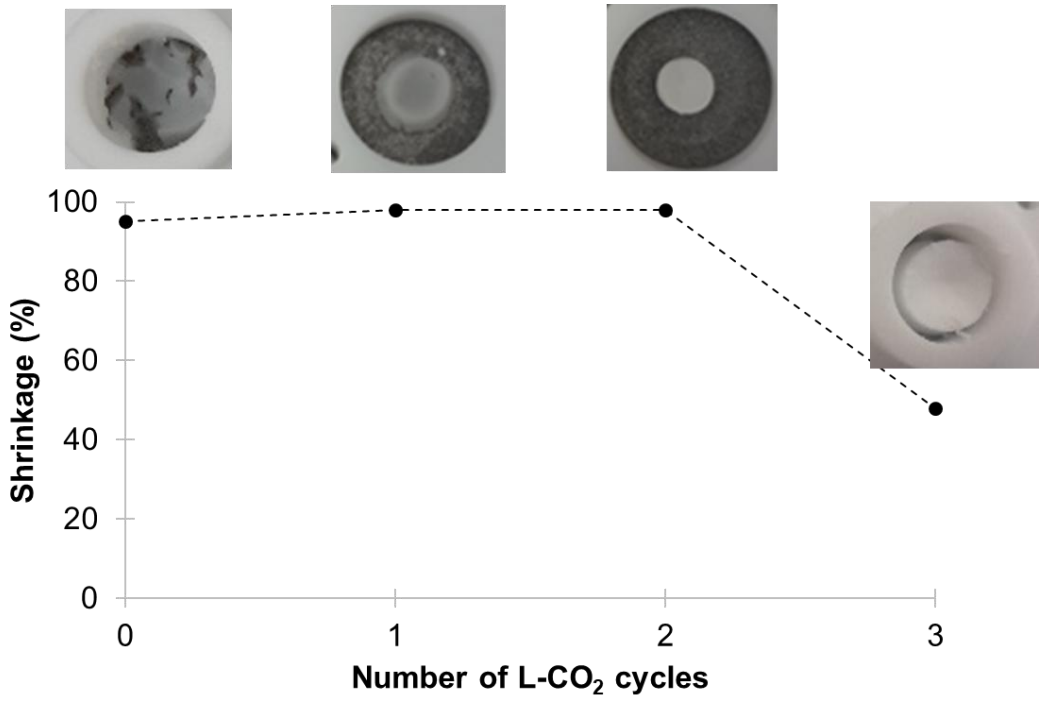

Fig. 2 Evolution of aerogel shrinkage with the increasing number of cycles in L-CO_2.

In the literature, no or little indication on the time and L-CO_2 flushes are given concerning the solvent exchange procedure (Hoepfner, Ratke, & Milow, 2008; Yiwen Li, Jiang, Han, & Zhang, 2019; Peng, Gardner, & Han, 2012; Sehaqui, Zhou, Ikkala, & Berglund, 2011). When mentioned into more details, long solvent exchange procedures for nanocellulose aerogel preparation have been reported by Buesch et al., (2016) and Zu et al., (2016) with solvent exchange steps in L-CO_2 lasting 12 hours and 1 day respectively. Here, the time necessary for the replacement of ethanol with L-CO_2 was reduced to 3 hours by using a minimum number of 3 successive L-CO_2 cycles. In this configuration, a maximum shrinkage of 48 % was observed for the less concentrated aerogels and drops to 12 % when the concentration is increased as will be discussed in the section. This optimization leads to time saving, cost-efficiency and reduced amount of CO_2 used.

3.2. Influence of preparation process and concentration on the macrostructure

Cryogels were produced from the ice-templating freeze-drying of a suspension of nanocellulose in water or after solvent exchange to *t*BuOH. Depending on the solvent, the resulting structures will be named CGw and CGtBuOH, when prepared from water and *t*BuOH, respectively. Aerogels were obtained after the process adaptation previously discussed. Both processes resulted in the production of white light solid foams as shown in Fig. 3. In the case of CNF-CGw, a flat, non-porous membrane is covering the structure. However, this phenomenon concerns a thin superficial layer on the outer surface of the sample but does not affect the global porosity.

TO-CNFs dried in supercritical conditions were the only one to yield transparent aerogels (Fig. 3e). This is the result of the combination of the small size TO-CNFs and the supercritical process maintaining a finer fibrillary network.

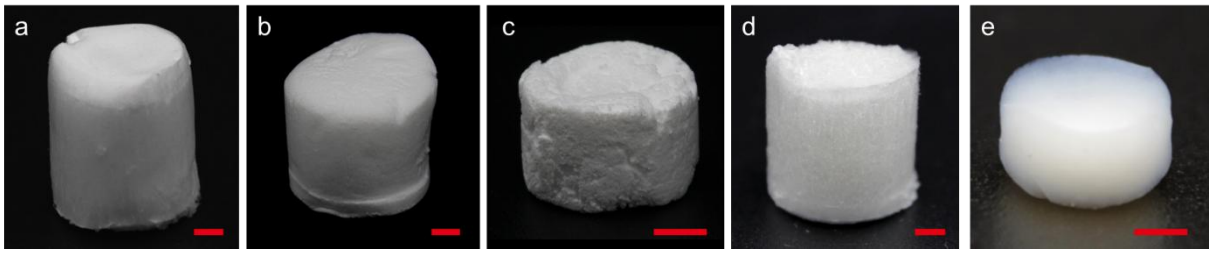

Fig. 3 Photographs of CNFs-CGw (a), CNFs-CGtBuOH (b), CNFs-AG (c), TO-CNFs-CGw (d) and TO-CNFs-AG (e). Scale bar represents 3 mm.

To evaluate the influence of the process on the macroscopic morphology, the initial suspension and the dry cryo- or aerogel volumes were reported and a volume shrinkage was deduced. Shrinkage of the porous foams was measured for samples prepared from suspensions of CNFs at different solid contents in water and *tert*-butyl alcohol for cryogels and in ethanol for aerogels. Results are presented as a function of concentration for the three types of porous foams: CNF-CGw, CNF-CGtBuOH and CNF-AG in Fig. 4.

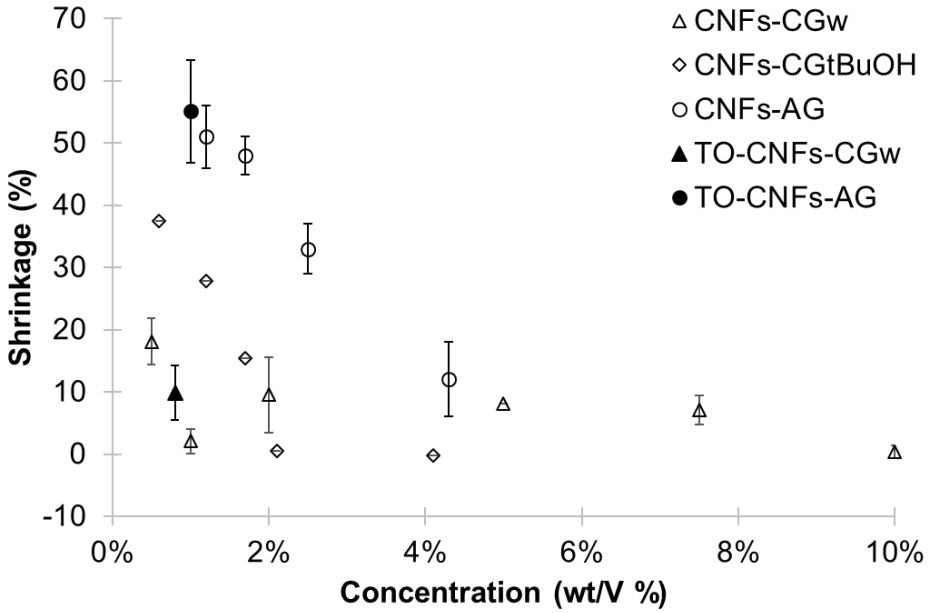

Fig. 4 Influence of concentration on the shrinkage at macroscopic scale of CGw cryogels (from water and tBuOH suspensions) and aerogels of CNFs. Shrinkage of TO-CNF cryogels is given at one concentration.

CNF cryogels prepared from the freeze-drying of a suspension in water exhibit low shrinkage even at low initial concentration of 0.5 (wt./vol.) % with less than 20 % volume shrinkage. For these

structures, shrinkage is independent of the concentration. There is a competition between the expansion of ice that is restricted with the increasing concentration and shrinkage due to pore collapse that is limited when the concentration increases and the pore walls thicken.

Oppositely, at low concentrations, CNF-CGtBuOH and CNF-AG exhibited high shrinkage of 38 and 51 % respectively. The volume reduction rapidly decreased for CNF-CGtBuOH to reach a minimum for a 2 (wt./vol.) % initial concentration. Aerogels also tend to present a reduced shrinkage when the concentration increases with as little as 12 % shrinkage for a 4 (wt/V) % solid content initial suspension. The decrease of shrinkage with concentration is noticeable for CNF-CGtBuOH and CNF-AG, structures that are dried after a solvent exchange step to a solvent (*t*BuOH or ethanol). The effect of concentration of volume shrinkage of aerogels was reported by Buchtová and Budtova (2016), who observed a decrease in shrinkage from 66 % to 21 % as the concentration of aerogel increases from 3% to 11 %, with dissolved cellulose. Similar values of shrinkage between 43 and 62 % were observed for CNC aerogels and shrinkage was attributed to the gel formation in acetone (Tripathi, Tardy, Khan, Liebner, & Rojas, 2019).

Shrinkage for TO-CNF cryogels was measured at one concentration and is close to values of shrinkage reported for both cryogels and aerogels of CNFs. We can therefore assume that shrinkage depends on the process and is independent on the nature of the nanocellulose.

3.3. Influence of preparation process on final porous structure for CNF materials

In order to understand the effect of the drying process on the final organization for both CNF and TO-CNF materials, the microscale morphology of cryogels and aerogels at 1 wt. % content was analyzed from SEM images presented in Fig. 5. Because of the difference of shrinkage induced by the different processes, different densities are reported: 10.2 ±0.2, 16.4 ± 0.4, 24.3 ± 1.7 $mg.cm^{-3}$ for CGw, CGtBuOH and AG prepared from CNFs, respectively, and 8.9 ± 0.4, 23.1 ± 4.3 $mg.cm^{-3}$ for CGw and AG prepared from TO-CNFs.

Cryogels freeze-dried from a suspension of CNFs in water exhibit a clear sheet-like organization due to the growth of ice-crystals during freezing. When the initial suspension is solvent exchanged to *tert*-butyl alcohol, the resulting CG_{tBuOH} cryogels exhibit a more fibrillary structure. Finally, aerogels present a highly fibrillary organization. Supercritical drying seems to preserve best the cellulose nanofibrils network and gives rise to the finest architectural structure. The difference between TO-CNF cryogels and aerogels is striking. Cryogels present large pores separated with dense sheets of TO-CNFs and the formation of ice-crystals is very obvious. On the other hand, TO-CNF aerogels appear to have a very smooth organization and when zoomed-in, the structure reveals a very fine and fibrillary arrangement. The supercritical drying has very well preserved the nanofibrils network.

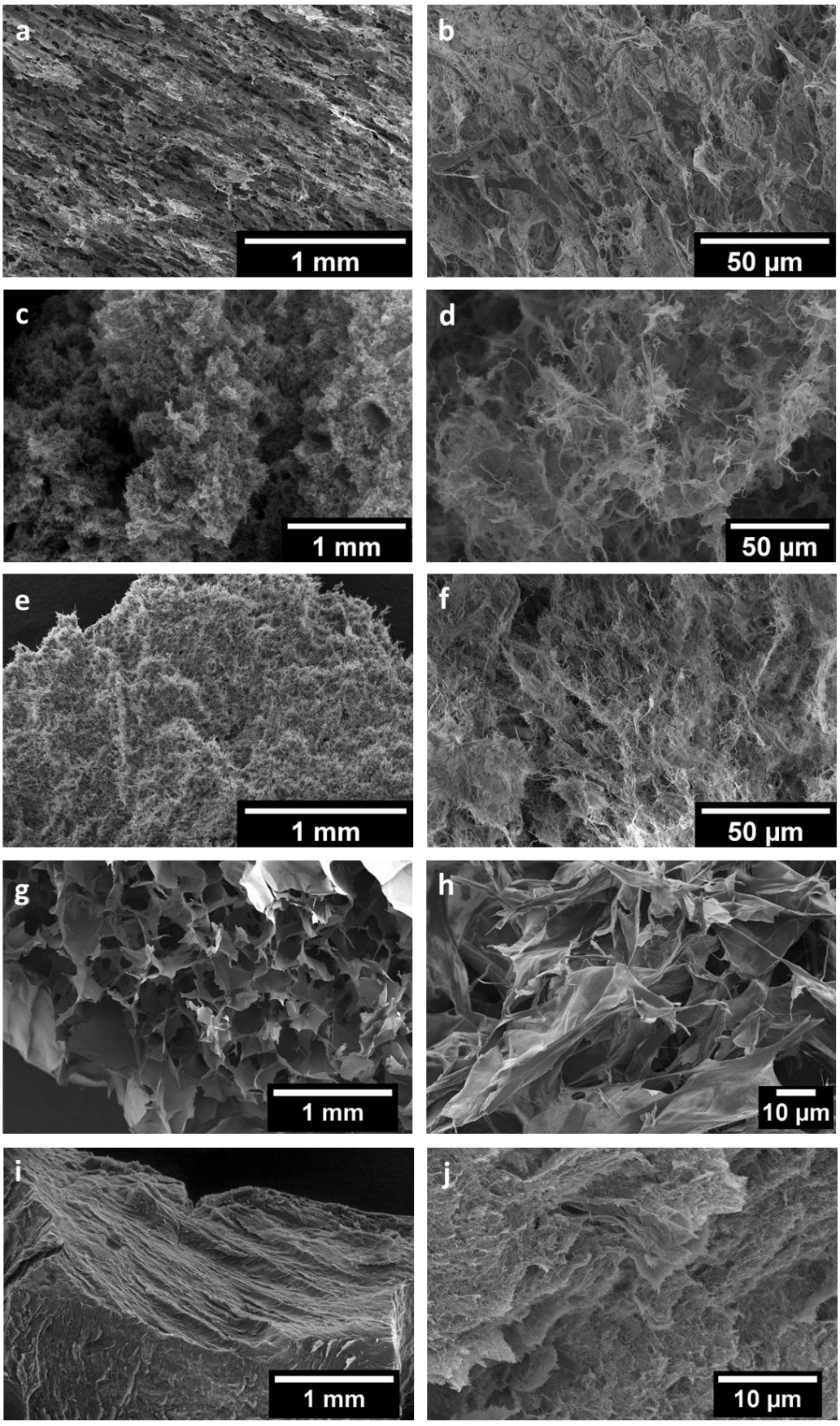

Fig. 5 SEM images of CNF-CGw (a, b), CNF-CGtBuOH (c, d), CNF-AG (e, f), TO-CNF-CGw (g, h), TO-CNF-AG (i, j).

From SEM images, micron-sized pores are analyzed and the pore size distributions are plotted in Fig. 6. Large pores are observed for the three types of porous structures obtained with CNFs. Such macropores are expected for cryogels as the drying process involves a freezing step during which ice-crystals can grow and form large pores. This is also true for CGtBuOH because of the presence of water in the mixture (20wt./wt. %). However, the solvent exchange to *t*BuOH gives rise to cryogel with a reduced amount of pores. Average pore sizes for CNF-CGw and CNF-CGtBuOH are of 17.8 ± 13.9 and 18.0 ± 9.6 µm, respectively. Martoïa et al. (2016) showed that the freezing rate greatly influences the crystals sizes. In their study, large pore diameters between 300 and 50 µm were observed at freezing temperature of -13°C and smaller pores of 20 to 10 µm were formed at lower freezing temperature of -80°C. These observations are consistent with measured radial pore sizes predominantly between 3 and 35 µm for cryogels prepared at -50°C. Few very large pores (up to 400 µm) are nevertheless observed in CG_w. In the case of aerogels, radial pore sizes are lower than for cryogels, ranging mainly between 1 and 15 µm with a mean pore diameter is of 8.8 ± 5.1 µm. For a same surface area studied, there are half the amount of pores observed for CGw.

TO-CNF cryogels exhibit typical radial pore sizes, of 24.7 ± 10.4 µm in average. The pores observed are larger, hence less numerous than for the same drying process with CNFs. A remarkable difference is observed with TO-CNF aerogels that present 50-fold smaller pores of 0.5 ± 0.2 µm. This result is attributed to the very homogeneous and small-sized TO-CNF particles combined to the supercritical drying process.

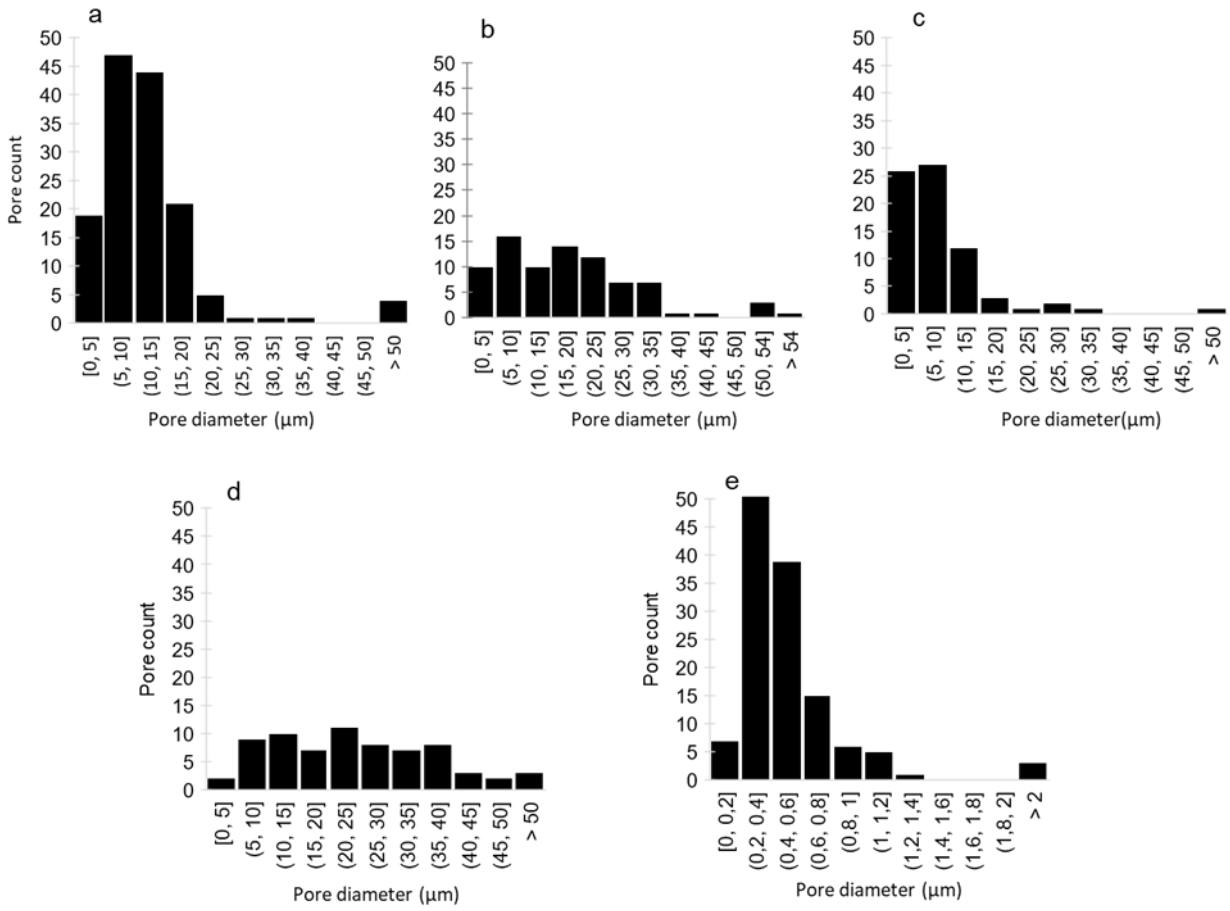

Fig. 6 Pore counts and size distribution of CNF-CGw (a), CNF-CGtBuOH (b), CNF-AG (c), TO-CNF-CGw (d) and TO-CNF-AG (e). Determined from electron microscopy images analysis of identical surface areas.

3.4. Influence of preparation process and concentration on the specific surface area

To study the influence of the preparation process on the properties of the resulting porous structures, nitrogen adsorption experiments were carried out on cryogels and aerogels of the two suspensions of nanocellulose. The gas pressure was increased to form a monolayer of nitrogen, adsorbed on the surface of the nanocellulose materials and the BET method was applied to determine the specific surface area of each structure. The calculated specific surface areas are plotted in Fig. 7 as a function of the initial concentration for CNF and at 1.5 % for TO-CNF structures.

Cryogels prepared from a suspension of CNFs in water have a specific surface area between 20 and 30 $m^2.g^{-1}$. The low standard deviation indicates the accuracy of this method and results. Similar results have been reported for CNF cryogels by Pääkkö et al. (2008), Xiao et al. (2015), Li et al. (2017) with values of specific surface area of 66, 20 and 31 $m^2.g^{-1}$, respectively. When CNFs are solvent exchanged to *tert*-butyl alcohol and freeze-dried, the resulting CGtBuOH show an increased specific surface area to around 100 $m^2.g^{-1}$. Contrary to CGw, more individual fibers remain, therefore increasing the specific surface area of the cryogel. Specific surface area increase after solvent

363 exchange was observed for oxidized cellulose nanofibrils (Sakai et al., 2016) and higher values for
364 cryogels obtained after solvent exchange are commonly reported (Fumagalli et al., 2013; Jin et al.,
365 2004; Sehaqui, Zhou, & Berglund, 2011). For both type of cryogels, the increasing concentration does
366 not affect the specific surface area of the prepared porous structure either.

367 Supercritical drying is well-known for preserving the structure of materials and avoiding pore
368 collapse and appears as the best method to produce foams with the highest specific surface area.
369 The CNF aerogels exhibit specific surface areas between 130 and 160 $m^2.g^{-1}$. These values are higher
370 than those reported by Ciftci et al. (2017). Moreover, no influence of the concentration was observed
371 here, while Ciftci et al. (2017) observed a reduction from 115 to 72 $m^2.g^{-1}$ when the concentration
372 increased from 1 to 2 wt. %.

373 For CNF cryogels and aerogels, no influence of the concentration was observed and in the case of
374 TO-CNF aerogels, Sakai et al., (2016) have shown that the specific surface area is also independent of
375 the concentration. At 1 % concentration, while TO-CNF cryogels exhibited a very low specific surface
376 area of 5 ±2 $m^2.g^{-1}$, aerogels feature very high specific surface area of 482 ± $m^2.g^{-1}$. This value is
377 amongst the highest reported in the literature, illustrating the great interest of supercritical drying of
378 oxidized cellulose. Very few papers discuss the production of TO-CNFs aerogels in supercritical
379 conditions. Sakai et al. (2016) prepared freeze-dried cryogels with a specific surface area of 20 $m^2.g^{-1}$
380 and aerogels with specific surface areas increased to 300-350 $m^2.g^{-1}$.

381 The highest specific surface areas were achieved with dissolved oxidized cellulose by Kobayashi,
382 Saito, & Isogai, (2014) who reported specific surface areas of 500-600 $m^2.g^{-1}$ for liquid crystalline
383 oxidized nanocellulose. Dissolved TO-CNFs-polypyrrole composites exhibited specific surface area of
384 246 $m^2.g^{-1}$ (O. Carlsson et al. 2012). Sehaqui et al. (2011b) prepared TO-CNFs nanopaper by critical
385 point drying with specific surface area of 482 $m^2.g^{-1}$. The prepared nanopapers differ from aerogels in
386 the sense that they are 2D materials and not highly porous as aerogels. Here, we prepared highly
387 porous aerogel from oxidized cellulose nanofibrils with the highest specific surface areas.

388

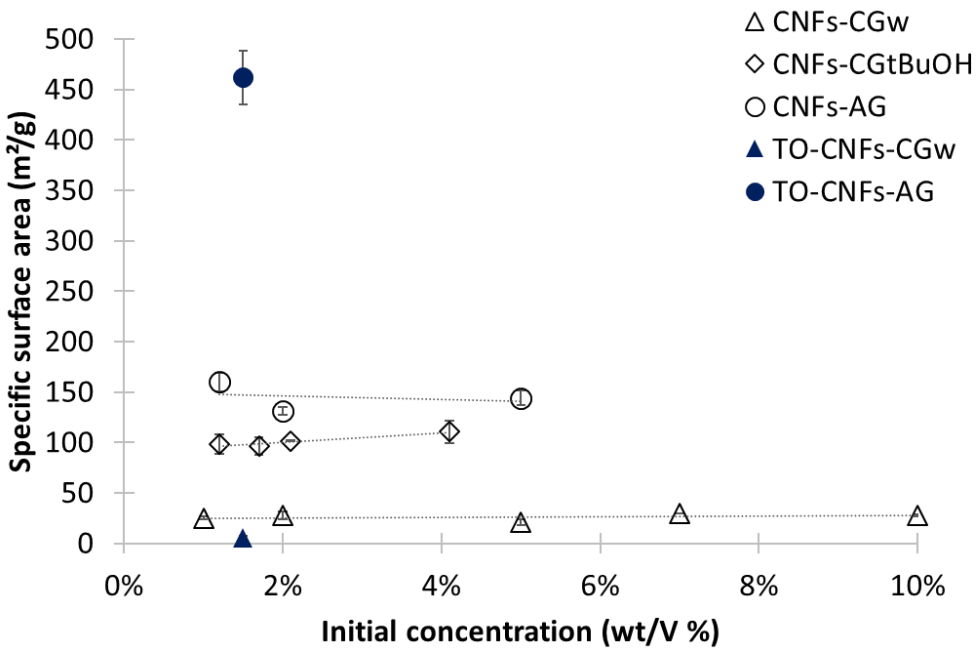

Fig. 7 Influence of the preparation process and the initial concentration on the specific surface area of cryogels and aerogels of CNFs and value of specific surface area of cryogels and aerogels of TO-CNFs at a given concentration.

3.5. Water uptake capacity

The water uptake capacity of the cryogels and aerogels was studied for CNF and TO-CNF materials, in water and in PBS. This buffer solution is used to simulate human body conditions in term of ion concentration and osmolarity. Results are presented in Fig. 8.

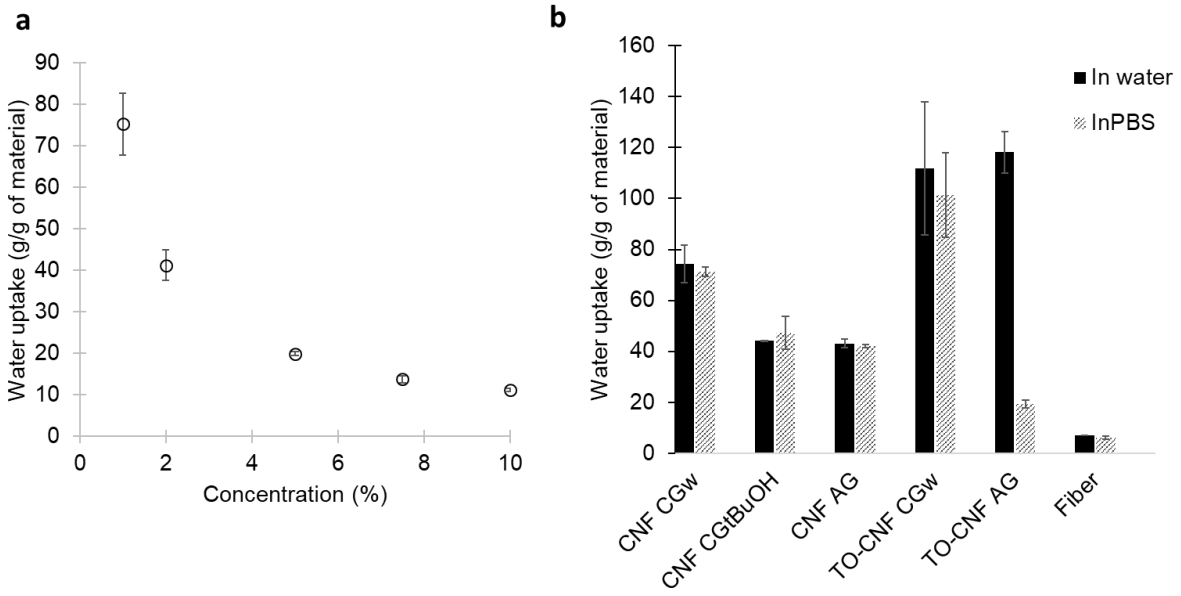

Fig. 8 Influence of the concentration on the water uptake of CNF cryogels (CGw) (a) and water uptake of different nanocellulose structures in water and PBS (b).

First, the water uptake in gram of water per gram of material was studied for CNF cryogels at increasing concentrations, and the relationship is presented in Fig. 8a. With increasing concentration, the amount of water retained decreases in a linear trend at first, which then appears to stabilize. The densest cryogels (10 wt. %) retain up to 11 g of water per gram of CNFs. As the density increases, more fibrils- fibrils interactions are created, CNFs form more hydrogen bonds with themselves than with water molecules, hence the decreased water uptake as the concentration increases.

In Fig. 8b, the water uptake for the different porous materials is presented for both immersion in water and in PBS. The water uptake for CNFs materials is slightly higher for CGw than for CGtBuOH and aerogels. Although no striking difference is observed, this variation could be due to the slightly higher density of the structures that undergo solvent exchange in their preparation process, from 10.2 for CGw to 16.4 and 24.3 $mg.cm^{-3}$ for CGtBuOH and AG, respectively. Overall, the preparation process has little or no incidence on the water uptake of the resulting material.

However, when TO-CNF structures are compared to CNF structures, a meaningful in water uptake is observed for oxidized CNFs materials. TO-CNF cryogels and aerogels exhibit water uptake of 113 and 119, respectively. This behavior is linked to the large amount of carboxyl groups, making the nanofibrils more hydrophilic. The presence of carboxyl groups also improves the materials' wet mechanical holding and a real hydrogel is formed. The mechanical holding of structures in water was observed after 2 hours in water under 75 ppm shaking and images are reported in supplementary material, Fig. A3. The mechanical holding after water uptake is poor for CNF structures obtained from supercritical drying and freeze-drying of a suspension in *t*BuOH. Those structures underwent a solvent exchange step. The observation of thinner pore walls for the structures (AG and CGtBuOH) can explain why the structure is more prone to collapse when humid. During cryogels (CGw) preparation, there is formation of a thick layer, with little porosity, surrounding the materials. More fibrils-fibrils interactions (H-bonds) are created around the materials, leading to a better preserved structure in wet conditions.

The water uptake of CNF structures is similar in water and PBS. On the other hand, a decrease is observed for TO-CNF structures in PBS, especially important for the TO-CNF aerogel, for which a drop from 119 to 19 is reported. The ions and salinity of the phosphate buffered saline solution are likely to screen the charged carboxyl groups. The presence of monovalent ions will induce attractive interactions between the fibrils, as explained by the DLVO theory. In the presence of multivalent ions, more complex mechanisms of attractive interaction between the fibrils apply (Benselfelt, Nordenström, Lindström, & Wågberg, 2019). The water molecules are less likely to bind with the TO-

CNFs, hence a lower water uptake. The differences observed between TO-CNF CGw and AG are linked to the higher density of AG (due to higher shrinkage) which further limits the water uptake due to a greater amount of interactions. Finally, the water uptakes of the different structures were compared to cellulose fibers that only gain 7 and 5 times their own weight in water and PBS, respectively. The very low water uptakes highlight the importance of the nano-sized fibrils and the porous architecture.

Capillary water uptake on skin mimicking layers was perform in order to be closer to in vivo conditions. A set-up with a hypodermis and a dermis mimicking layer is prepared as illustrated in Fig. 9a and b. Cryogels and aerogels are placed on the top layer mimicking the dermis. The hypodermis underneath is more humid and prevents the drying of the top dermis layer during the experiment. The results are presented in Fig. 9c and d.

A rapid water uptake is observed for every structure during the first 6 hours. After a rapid uptake of the structure, the water uptake speed decreases and stabilizes along time. Speeds are deduced from the curve slopes and are reported in supplementary material, Table A1. The capillary water uptake speeds appear to be steady for long periods of time (up to one week). The water uptake behavior is similar to what is observed from immersion experiments, although values are much lower due to the lower availability of water in the gelatin/agar layers.

A faster and greater water uptake is observed for TO-CNF cryogels and aerogels. CNF structures present similar water uptake rate for both cryogels and aerogels, and the overall water uptake is lower and slower when compared to TO-CNF structures. The porous materials are good candidates for wound dressings applications to absorb large amounts of exudate. Depending on the type of nanocellulose and the drying conditions, the water uptake capacities are tunable.

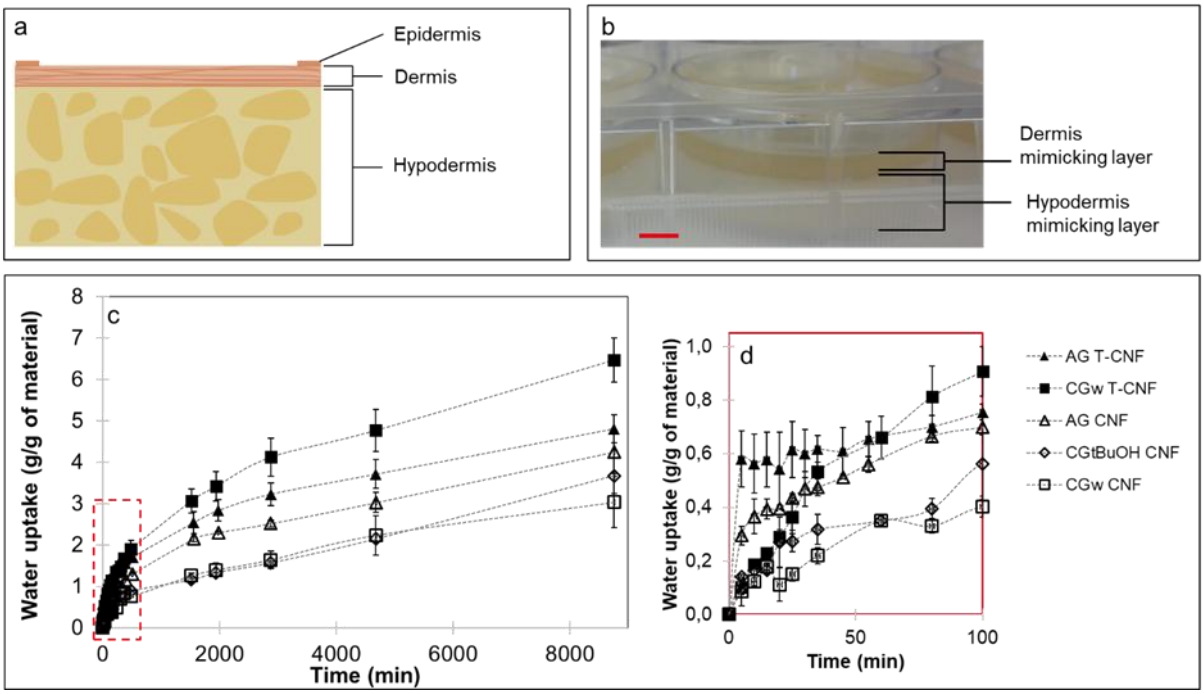

Fig. 9 Schematic representation of skin with ruptured epidermis (a), photograph of skin mimicking layers of hypodermis and dermis, the scale bar is 10 mm (b), capillary water uptake kinetics of CNFs and TO-CNFs cryogels and aerogels (c) and zoomed-in graph (d)

4. Conclusion

The formation of highly porous, low density and high specific surface area cellulose nanofibrils structures was investigated. Different drying methods, namely freeze-drying and supercritical drying have been adopted and the resulting effect on the macro and micro-structure was investigated. The initial suspension concentration influences the final macroscopic morphology. Although volume shrinkage was significant for structures obtained from *tert*-butyl alcohol freeze-drying and supercritical drying, it decreased rapidly when the initial concentration was increased. The pore size distribution was affected by the process, as well as the specific surface areas which varied from 25 $m^2.g^{-1}$ for cryogels to 160 $m^2.g^{-1}$ for aerogels. Oxidized cellulose nanofibrils structured were compared to non-oxidized CNFs structures. Very high specific surface area aerogels where obtained, with values of 482 $m^2.g^{-1}$ among the highest reported for CNF-only aerogels. The microscopic scale analysis exhibited aerogels with very fine and preserved fibrillary network and microporosity. The water uptake experiments demonstrated excellent water uptake capacities of TO-CNF structures as well as excellent wet holding mechanical behavior. The different results depending on the nanocellulose chemistry and the porous material preparation process suggest a possible use of the produced aerogels for wound dressing applications where exudate removal is essential or for humidity control of a moist environment.

Acknowledgments

This work was supported by a grant from Labex ARCANE (ANR-11-LABX-0003-01) and CBH-EUR-GS (ANR-17-EURE-0003) and supported by the “Investissement d’avenir” program Glyco@Alps (ANR-15-IDEX-02). The authors acknowledge the Borregaard company for providing CNF materials and thank Jean-Luc Putaux and Christine Lancelon-Pin for the microscopy images. LGP2 is part of the LabEx Tec 21 (Investissements d’Avenir—Grant Agreement No. ANR-11-LABX-0030) and of PolyNat Carnot Institute (Investissements d’Avenir—Grant Agreement No. ANR-16-CARN-0025-01).

References

Benselfelt, T., Nordenström, M., Lindström, S. B., & Wågberg, L. (2019). Explaining the Exceptional Wet Integrity of Transparent Cellulose Nanofibril Films in the Presence of Multivalent Ions—Suitable Substrates for Biointerfaces. *Advanced Materials Interfaces*, *6*(13), 1900333. https://doi.org/10.1002/admi.201900333

Besbes, I., Alila, S., & Boufi, S. (2011). Nanofibrillated cellulose from TEMPO-oxidized eucalyptus fibres: Effect of the carboxyl content. *Carbohydrate Polymers*, *84*(3), 975–983. https://doi.org/10.1016/j.carbpol.2010.12.052

Brunauer, S., Emmett, P. H., & Teller, E. (1938). Adsorption of Gases in Multimolecular Layers. *Journal of the American Chemical Society*, *60*(2), 309–319. https://doi.org/10.1021/ja01269a023

Buchtová, N., & Budtova, T. (2016). Cellulose aero-, cryo- and xerogels: towards understanding of morphology control. *Cellulose*, *23*(4), 2585–2595. https://doi.org/10.1007/s10570-016-0960-8

Buesch, C., Smith, S. W., Eschbach, P., Conley, J. F., & Simonsen, J. (2016). The Microstructure of Cellulose Nanocrystal Aerogels as Revealed by Transmission Electron Microscope Tomography. *Biomacromolecules*, *17*(9), 2956–2962. https://doi.org/10.1021/acs.biomac.6b00764

Chen, A. I., Balter, M. L., Chen, M. I., Gross, D., Alam, S. K., Maguire, T. J., & Yarmush, M. L. (2016). Multilayered tissue mimicking skin and vessel phantoms with tunable mechanical, optical, and acoustic properties. *Medical Physics*, *43*(6), 3117–3131. https://doi.org/10.1118/1.4951729

Ciftci, D., Ubeyitogullari, A., Huerta, R. R., Ciftci, O. N., Flores, R. A., & Saldaña, M. D. A. (2017). Lupin hull cellulose nanofiber aerogel preparation by supercritical CO 2 and freeze drying. *The Journal of Supercritical Fluids*, *127*, 137–145. https://doi.org/10.1016/j.supflu.2017.04.002

508 Desmaisons, J., Boutonnet, E., Rueff, M., Dufresne, A., & Bras, J. (2017). A new quality index for
509 benchmarking of different cellulose nanofibrils. *Carbohydrate Polymers*, *174*, 318–329.
510 https://doi.org/10.1016/j.carbpol.2017.06.032
511 Fumagalli, M., Sanchez, F., Molina Boisseau, S., & Heux, L. (2013). Gas-phase esterification of
512 cellulose nanocrystal aerogels for colloidal dispersion in apolar solvents. *Soft Matter*, *9*(47),
513 11309–11317. https://doi.org/10.1039/C3SM52062E
514 García-González, C. A., Camino-Rey, M. C., Alnaief, M., Zetzl, C., & Smirnova, I. (2012). Supercritical
515 drying of aerogels using CO2: Effect of extraction time on the end material textural
516 properties. *The Journal of Supercritical Fluids*, *66*, 297–306.
517 https://doi.org/10.1016/j.supflu.2012.02.026
518 Han, Y., Zhang, X., Wu, X., & Lu, C. (2015). Flame Retardant, Heat Insulating Cellulose Aerogels from
519 Waste Cotton Fabrics by in Situ Formation of Magnesium Hydroxide Nanoparticles in
520 Cellulose Gel Nanostructures. *ACS Sustainable Chemistry & Engineering*, *3*(8), 1853–1859.
521 https://doi.org/10.1021/acssuschemeng.5b00438
522 Heath, L., & Thielemans, W. (2010). Cellulose nanowhisker aerogels. *Green Chemistry*, *12*(8), 1448.
523 https://doi.org/10.1039/c0gc00035c
524 Hoepfner, S., Ratke, L., & Milow, B. (2008). Synthesis and characterisation of nanofibrillar cellulose
525 aerogels. *Cellulose*, *15*(1), 121–129. https://doi.org/10.1007/s10570-007-9146-8
526 Jin, H., Nishiyama, Y., Wada, M., & Kuga, S. (2004). Nanofibrillar cellulose aerogels. *Colloids and*
527 *Surfaces A: Physicochemical and Engineering Aspects*, *240*(1–3), 63–67.
528 https://doi.org/10.1016/j.colsurfa.2004.03.007
529 Jorfi, M., & Foster, E. J. (2015). Recent advances in nanocellulose for biomedical applications. *Journal*
530 *of Applied Polymer Science*, *132*(14), n/a-n/a. https://doi.org/10.1002/app.41719
531 Klemm, D., Cranston, E. D., Fischer, D., Gama, M., Kedzior, S. A., Kralisch, D., … Rauchfuß, F. (2018).
532 Nanocellulose as a natural source for groundbreaking applications in materials science:

Today's state. *Materials Today*, *21*(7), 720–748. https://doi.org/10.1016/j.mattod.2018.02.001

Kobayashi, Y., Saito, T., & Isogai, A. (2014). Aerogels with 3D Ordered Nanofiber Skeletons of Liquid-Crystalline Nanocellulose Derivatives as Tough and Transparent Insulators. *Angewandte Chemie International Edition*, *53*(39), 10394–10397. https://doi.org/10.1002/anie.201405123

Korhonen, J. T., Hiekkataipale, P., Malm, J., Karppinen, M., Ikkala, O., & Ras, R. H. A. (2011). Inorganic Hollow Nanotube Aerogels by Atomic Layer Deposition onto Native Nanocellulose Templates. *ACS Nano*, *5*(3), 1967–1974. https://doi.org/10.1021/nn200108s

Li, Yinyong, Tanna, V. A., Zhou, Y., Winter, H. H., Watkins, J. J., & Carter, K. R. (2017). Nanocellulose Aerogels Inspired by Frozen Tofu. *ACS Sustainable Chemistry & Engineering*, *5*(8), 6387–6391. https://doi.org/10.1021/acssuschemeng.7b01608

Li, Yiwen, Jiang, H., Han, B., & Zhang, Y. (2019). Drying of cellulose nanocrystal gel beads using supercritical carbon dioxide. *Journal of Chemical Technology & Biotechnology*, *94*(5), 1651–1659. https://doi.org/10.1002/jctb.5936

Liebner, F., Haimer, E., Wendland, M., Neouze, M.-A., Schlufter, K., Miethe, P., … Rosenau, T. (2010). Aerogels from Unaltered Bacterial Cellulose: Application of scCO2 Drying for the Preparation of Shaped, Ultra-Lightweight Cellulosic Aerogels. *Macromolecular Bioscience*, *10*(4), 349–352. https://doi.org/10.1002/mabi.200900371

Martoïa, F., Cochereau, T., Dumont, P. J. J., Orgéas, L., Terrien, M., & Belgacem, M. N. (2016). Cellulose nanofibril foams: Links between ice-templating conditions, microstructures and mechanical properties. *Materials & Design*, *104*, 376–391. https://doi.org/10.1016/j.matdes.2016.04.088

Nechyporchuk, O., Belgacem, M. N., & Bras, J. (2016). Production of cellulose nanofibrils: A review of recent advances. *Industrial Crops and Products*, *93*, 2–25. https://doi.org/10.1016/j.indcrop.2016.02.016

558 Nyström, G., Marais, A., Karabulut, E., Wågberg, L., Cui, Y., & Hamedi, M. M. (2015). Self-assembled
559 three-dimensional and compressible interdigitated thin-film supercapacitors and batteries.
560 *Nature Communications*, *6*(1). https://doi.org/10.1038/ncomms8259
561 O. Carlsson, D., Nyström, G., Zhou, Q., A. Berglund, L., Nyholm, L., & Strømme, M. (2012).
562 Electroactive nanofibrillated cellulose aerogel composites with tunable structural and
563 electrochemical properties. *Journal of Materials Chemistry*, *22*(36), 19014–19024.
564 https://doi.org/10.1039/C2JM33975G
565 Pääkkö, M., Ankerfors, M., Kosonen, H., Nykänen, A., Ahola, S., Österberg, M., … Lindström, T. (2007).
566 Enzymatic Hydrolysis Combined with Mechanical Shearing and High-Pressure
567 Homogenization for Nanoscale Cellulose Fibrils and Strong Gels. *Biomacromolecules*, *8*(6),
568 1934–1941. https://doi.org/10.1021/bm061215p
569 Pääkkö, Marjo, Vapaavuori, J., Silvennoinen, R., Kosonen, H., Ankerfors, M., Lindström, T., … Ikkala,
570 O. (2008). Long and entangled native cellulose I nanofibers allow flexible aerogels and
571 hierarchically porous templates for functionalities. *Soft Matter*, *4*(12), 2492.
572 https://doi.org/10.1039/b810371b
573 Peng, Y., Gardner, D. J., & Han, Y. (2012). Drying cellulose nanofibrils: in search of a suitable method.
574 *Cellulose*, *19*(1), 91–102. https://doi.org/10.1007/s10570-011-9630-z
575 Saito, T., & Isogai, A. (2004). TEMPO-Mediated Oxidation of Native Cellulose. The Effect of Oxidation
576 Conditions on Chemical and Crystal Structures of the Water-Insoluble Fractions.
577 *Biomacromolecules*, *5*(5), 1983–1989. https://doi.org/10.1021/bm0497769
578 Saito, T., Nishiyama, Y., Putaux, J.-L., Vignon, M., & Isogai, A. (2006). Homogeneous Suspensions of
579 Individualized Microfibrils from TEMPO-Catalyzed Oxidation of Native Cellulose.
580 *Biomacromolecules*, *7*(6), 1687–1691. https://doi.org/10.1021/bm060154s
581 Sakai, K., Kobayashi, Y., Saito, T., & Isogai, A. (2016). Partitioned airs at microscale and nanoscale:
582 thermal diffusivity in ultrahigh porosity solids of nanocellulose. *Scientific Reports*, *6*(1).
583 https://doi.org/10.1038/srep20434

584 Sanz-Moral, L. M., Rueda, M., Mato, R., & Martín, Á. (2014). View cell investigation of silica aerogels
585 during supercritical drying: Analysis of size variation and mass transfer mechanisms. *The*
586 *Journal of Supercritical Fluids*, *92*, 24–30. https://doi.org/10.1016/j.supflu.2014.05.004
587 Sehaqui, H., Zhou, Q., & Berglund, L. A. (2011). High-porosity aerogels of high specific surface area
588 prepared from nanofibrillated cellulose (NFC). *Composites Science and Technology*, *71*(13),
589 1593–1599. https://doi.org/10.1016/j.compscitech.2011.07.003
590 Sehaqui, H., Zhou, Q., Ikkala, O., & Berglund, L. A. (2011). Strong and Tough Cellulose Nanopaper with
591 High Specific Surface Area and Porosity. *Biomacromolecules*, *12*(10), 3638–3644.
592 https://doi.org/10.1021/bm2008907
593 Stergar, J., & Maver, U. (2016). Review of aerogel-based materials in biomedical applications. *Journal*
594 *of Sol-Gel Science and Technology*, *77*(3), 738–752. https://doi.org/10.1007/s10971-016-
595 3968-5
596 Tripathi, A., Tardy, B. L., Khan, S. A., Liebner, F., & Rojas, O. J. (2019). Expanding the upper limits of
597 robustness of cellulose nanocrystal aerogels: outstanding mechanical performance and
598 associated pore compression response of chiral-nematic architectures. *Journal of Materials*
599 *Chemistry A*. https://doi.org/10.1039/C9TA03950C
600 Xiao, S., Gao, R., Lu, Y., Li, J., & Sun, Q. (2015). Fabrication and characterization of nanofibrillated
601 cellulose and its aerogels from natural pine needles. *Carbohydrate Polymers*, *119*, 202–209.
602 https://doi.org/10.1016/j.carbpol.2014.11.041
603 Zhang, X., Yu, Y., Jiang, Z., & Wang, H. (2015). The effect of freezing speed and hydrogel
604 concentration on the microstructure and compressive performance of bamboo-based
605 cellulose aerogel. *Journal of Wood Science*, *61*(6), 595–601. https://doi.org/10.1007/s10086-
606 015-1514-7
607 Zhou, S., Liu, P., Wang, M., Zhao, H., Yang, J., & Xu, F. (2016). Sustainable, Reusable, and
608 Superhydrophobic Aerogels from Microfibrillated Cellulose for Highly Effective Oil/Water

609 Separation. *ACS Sustainable Chemistry & Engineering*, *4*(12), 6409–6416.
610 https://doi.org/10.1021/acssuschemeng.6b01075
611 Zu, G., Shen, J., Zou, L., Wang, F., Wang, X., Zhang, Y., & Yao, X. (2016). Nanocellulose-derived highly
612 porous carbon aerogels for supercapacitors. *Carbon*, *99*, 203–211.
613 https://doi.org/10.1016/j.carbon.2015.11.079

614